Highly transparent conductive ITO/Ag/ITO trilayer films deposited by RF sputtering at room temperature

Ningyu Ren, Jun Zhu,[a] and Shiliang Ban[a]
School of Physical Science and Technology, Inner Mongolia University, Key Laboratory of Semiconductor Photovoltaic Technology at Universities of Inner Mongolia Autonomous Region, Hohhot 010021, People's Republic of China

(Received 20 February 2017; accepted 20 April 2017; published online 16 May 2017)

ITO/Ag/ITO (IAI) trilayer films were deposited on glass substrate by radio frequency magnetron sputtering at room temperature. A high optical transmittance over 94.25% at the wavelength of 550 nm and an average transmittance over the visual region of 88.04% were achieved. The calculated value of figure of merit (FOM) reaches 80.9 10^{-3} Ω^{-1} for IAI films with 15-nm-thick Ag interlayer. From the morphology and structural characterization, IAI films could show an excellent correlated electric and optical performance if Ag grains interconnect with each other on the bottom ITO layer. These results indicate that IAI trilayer films, which also exhibit low surface roughness, will be well used in optoelectronic devices. [http://dx.doi.org/10.1063/1.4982919]

I. INTRODUCTION

Transparent conductive films (TCFs) are essential for photosensitive electronic devices such as thin film solar cells, flat panel displays, touch screens, organic light-emitting diodes and so on.[1] Usually, there are at least two important factors to evaluate the performance of TCF depending on its special application. First, low sheet resistance is needed especially when TCF is used as electrode material. Next, high optical transmittance in the visual spectrum is another important characteristic of a high-quality TCF. Due to the great advance of experimental exploration, a large variety of TCFs, including traditional metal oxides,[2–7] graphene,[8] carbon nanotubes,[9] metal nanostructures,[10–14] and so on, have been successfully fabricated and widely applied in optoelectronic devices. Among these TCFs, tin-doped indium oxide (ITO) dominates the market in high-end optoelectronics because of its excellent electrical and optical properties. However, ITO suffers from high processing temperature, brittleness and thermal instability and is composed of the expensive rare element Indium.[15] In addition, it becomes very hard to further lower the sheet resistance by using single ITO film.

To overcome such limitations, multilayer TCFs, as one type of promising candidates, have been extensively investigated in recent decades. On one hand, the TCFs of bilayer structure, e.g., semiconductor/semiconductor[16–18] and semiconductor/metal[19–21] bilayer films, were studied by some authors. On the other hand, TCF/metal/TCF trilayer structures[22] were rapidly developed since they might provide optical and electrical characteristics superior to those single-layer or bilayer TCFs. Early report showed this dielectric-metal-dielectric structure could suppress the reflection from the metal layer in the visible region and achieve a selective transparent effect.[23] In this case, Ag, Cu, Au, Al and their alloys were often deposited between two metal oxide layers to form a sandwich-structure TCF stack.[22] A large number of transparent conductive oxides (TCOs), e.g., ZnO,[23,24] AZO,[25] MgZnO,[26] FTO,[27] WO_3,[28] ITO,[29] etc., were employed to improve the performance of trilayer TCFs.

In particular, ITO/Ag/ITO (IAI) trilayer films have been played more attention for its promising application in various optoelectronic devices. The electric and optical behaviors of IAI films strongly

[a]Corresponding authors: Jun Zhu, jiulye@126.com; Shiliang Ban, slban@imu.edu.cn

TABLE I. Deposition conditions for preparing IAI films.

Deposition parameter	ITO	Ag
Target	90% In_2O_3 and 10% SnO_2	Ag
The diameter of target	50 mm	50 mm
Target-to-substrate distance	70 mm	70 mm
Substrate	glass	glass
Substrate temperature	Room temperature	Room temperature
Base pressure	5×10^{-4} Pa	5×10^{-4} Pa
Sputtering medium	Ar (purity 99.99%)	Ar (purity 99.99%)
Gas flow	30 sccm	30 sccm
Working pressure	0.25 Pa	0.2 Pa

depend on the thicknesses and deposition conditions of Ag interlayer and ITO films. It is indicated that the Ag interlayer should be thin, continuous and incompletely coated on ITO bottom film for high transmittance and low resistance. Besides, a low-temperature process for TCFs is critically required for optoelectronic applications. So far, efforts by many groups[29–47] have led to significant improvement on the performance of IAI trilayer electrodes.

In this work, we studied the structural, electrical and optical properties of IAI trilayer thin films, which were sputtered on glass substrate at room temperature. The modification of morphology, crystal structure, sheet resistance and optical transmittance induced by the thicknesses of Ag interlayer as well as different ITO layers were discussed in detail. It is found that the IAI samples exhibits excellent optical and electric properties and the values of figure of merit (FOM) were calculated as much higher than most of previous reports.

II. EXPERIMENTAL

The substrates used here were soda lime glass in the size of 25 mm×30 mm. Before being loaded into the sputtering chamber, they were cooked in electronic cleaning agent for 30 min, and then ultrasonically cleaned in an acetone bath to remove organic and metallic contaminants, and ultrasonically cleaned in alcohol successively, cleaned by deionized water and finally dried in a N_2 stream. A ceramic ITO target (99.99% purity) with the composition of 90% indium oxide and 10% tin oxide by weight and a metallic Ag target (99.99% purity) were used in a RF magnetron sputtering system. The system is capable of obtaining a base vacuum of 5×10^{-4} Pa. The target-to-substrate distance is about 70 mm. Prior to deposition, both the ITO and Ag targets were pre-sputtered for 30 min to remove contaminants. The IAI trilayer thin films were successively deposited onto glass substrates. Firstly, the bottom ITO layer was deposited with a sputtering power of 30 W at a pressure of 0.25 Pa in a pure Ar atmosphere. After that, the Ag film was deposited under the condition of 0.2 Pa and 30 W. Finally, the top ITO layer was deposited onto the Ag interlayer under the same deposition conditions with that of the bottom ITO layer. It should be noticed that the chamber was vacuumed after each deposition process. The deposition rates of ITO and Ag film were evaluated as 0.2 nm/s and 0.5 nm/s, respectively. The deposition conditions in preparing each layer of IAI films are listed in Table I.

The surface morphology of as-deposited films was characterized by a field emission scanning electron microscope (SEM, S-3400, Hitachi) and an atomic force microscope (AFM, CSPM5500). The crystallographic structures and phases of the samples were determined by a transmission electron microscope (TEM, Tecnai f20, Fei). The standard four-point-probe technique was used to measure the sheet resistance of the samples. The optical transmittance of the films was measured by a UV/Visible (UV/Vis) spectrometer (Lambda 650, Perkin Elmer) and obtained by discounting the glass substrate.

III. RESULTS AND DISCUSSION

The schematic structure of IAI trilayer films deposited on glass substrate was depicted in Fig. 1 (a). The transmittance of the glass substrate was the same as that in Ref. 37. For comparison,

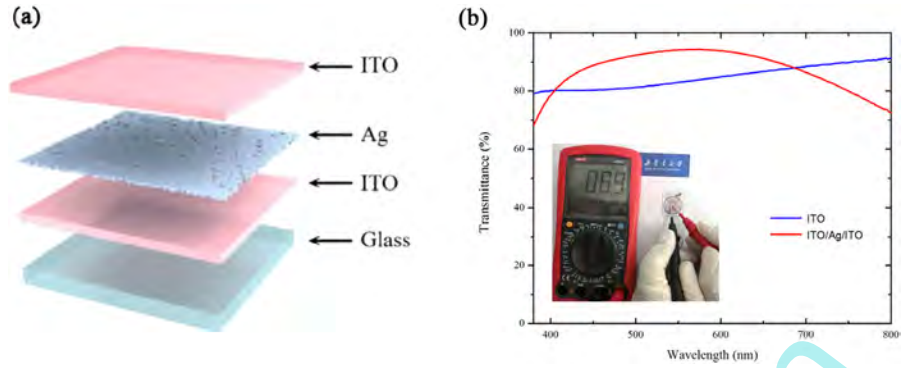

FIG. 1. (a) Schematic structure of the IAI multilayer films (b) Optical transmittance of ITO (48 nm) /Ag (12.5 nm) /ITO (42 nm) trilayer film and as-sputtered ITO (90 nm) single-layer film.

the optical transmittances of ITO (48 nm) /Ag (12.5 nm) /ITO (42 nm) trilayer film and as-sputtered ITO (90 nm) single-layer film were shown in Fig. 1 (b). As seen, the IAI trilayer films are possible to attain more excellent optical performance in the visual spectrum than single-layer ITO film despite of Ag interlayer. Table II gives the measured values of optical transmittance and sheet resistance for both samples in detail. The IAI films have a sheet resistance of 7.04 Ω/sq, an average optical transmittance of 88.04% between 400 and 800 nm, and an optical transmittance of 94.25% at 550 nm, which are significantly better than single-layer ITO film.

Fig. 2 (a) shows the optical transmittance of ITO (48 nm) /Ag/ITO (42 nm) trilayer films in the wavelength region from 400 to 800 nm as a function of the thickness d_{Ag} of Ag interlayer. It can be seen that when d_{Ag} changes from 12.5 to 17.5 nm, the films exhibit very good optical transmittance. Especially, if d_{Ag} = 12.5 nm, the sample has the highest optical transmittance over the visible region. However, the transmittance decreases as d_{Ag} further increases. In the case of d_{Ag} = 5 nm, the transmittance was comparatively low due to the light scattering on the isolated island-shaped Ag interlayer. In order to analyze the overall optical and electric properties of as-prepared IAI trilayer films, Fig. 2 (b) shows the optical transmittance at the wavelength of 550 nm, the sheet resistance and the FOM value of ITO (48 nm) /Ag/ITO (42 nm) trilayer films. It is clearly seen that the sheet resistance continuously decreases with d_{Ag} increasing from 5 nm. The sheet resistance of the IAI trilayer films can be estimated using the following equation $\frac{1}{R_{sIAI}} \approx \frac{1}{R_{sAg}} + \frac{2}{R_{sITO}}$, where R_{sIAI}, R_{sAg}, and R_{sITO} represent the sheet resistances of the IAI films, the Ag film, and the ITO layer, respectively. If the sheet resistance of ITO is much larger than that of Ag interlayer, the sheet resistance of the IAI films will be mainly determined by the Ag film. When d_{Ag} = 12.5 nm, the measured optical transmittance at 550 nm is 94.25%, which is very close to the calculated theoretical data 95.97%.[35] All the transmittance value exceeds 80% if d_{Ag} > 12.5 nm. As d_{Ag} increases from 12.5 to 20 nm, the transmittance monotonically decreases, whereas d_{Ag} decreases from 12.5 to 5 nm, the transmittance also decreases. The reason will be further explained combined with SEM images in Fig. 3.

The FOM, as defined by Haacke,[48] was calculated by the formula $\varphi = \frac{T^{10}}{R_s}$, in which T^{10} is the optical transmittance at 550 nm and R_s is the sheet resistance. From Fig. 2 (b), it can be seen that the maximum of FOM value (80.9 10^{-3} Ω^{-1}) of the IAI trilayer films was obtained at d_{Ag} = 15 nm. The IAI trilayer electrodes with Ag interlayer thickness between 12.5 and 17.5 nm have similar FOM values (78.59, 80.9 and 77.63×10^{-3} Ω^{-1}). However, the FOM value decreases sharply as d_{Ag} < 12.5 nm since the light scattering by island-shaped Ag layer degrades the optical transmittance of samples.

TABLE II. Sheet resistance and optical transmittance of IAI trilayer film and ITO single-layer film.

Sample	Sheet resistance (Ω/sq)	Average optical transmittance (%)	Optical transmittance at 550 nm (%)
IAI	7.04	88.04	94.25
ITO	90.4	85.05	83.03

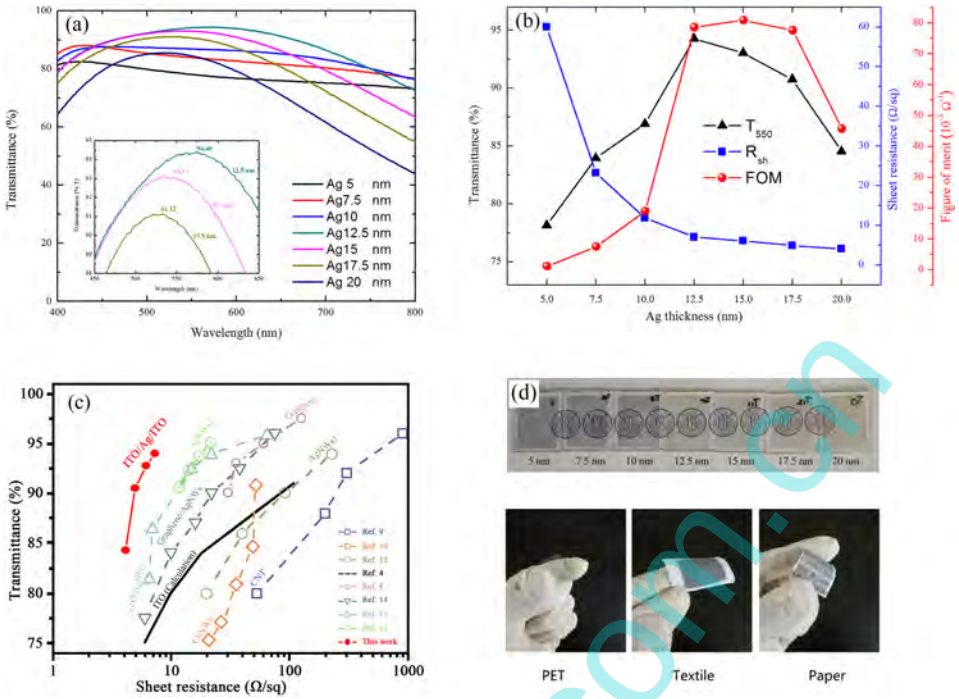

FIG. 2. (a) Optical transmittance of ITO (48 nm) /Ag/ITO (42 nm) films as a function of Ag thickness. (b) Optical transmittance at 550 nm, sheet resistance and FOM of ITO (48 nm) /Ag/ITO (42 nm) films as a function of Ag thickness. (c) Comparison of optical transmittance and sheet resistance in this work and other literatures. (d) ITO (48 nm) /Ag/ITO (42 nm) films on various flexible substrates including polyethylene terephthalate (PET), textile and paper.

In Fig. 2 (c), we further compare the optical and electric performance of our IAI trilayer films with that of other types of ITO candidates such as graphene, carbon-nanotube films, Ag and Cu nanowires. The best performance of our samples is 4.01 Ω/sq at T = 84.7%, 4.88 Ω/sq at T = 90.75%, 6.06 Ω/sq at T = 93.02%, and 7.04 Ω/sq at T = 94.25%, which is comparable to state-of-the-art device-grade ITO films and superior to other transparent conducting electrodes. Table III gives the maximum optical transmittance, minimum sheet resistance and largest FOM value of IAI trilayer films deposited on different substrates reported in the literature. It is clearly evident that the highest visible transmittance obtained in the present work is slightly higher than the previously reported values. The FOM value of

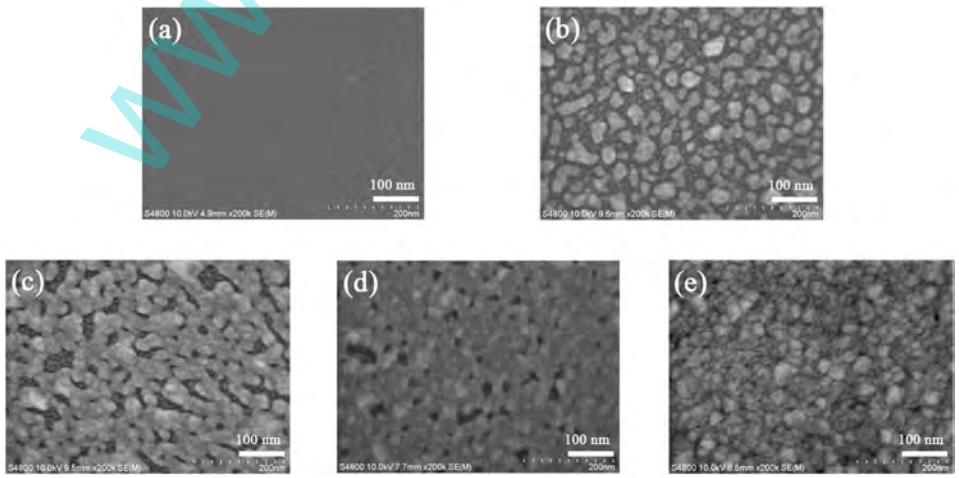

FIG. 3. Surface FESEM images of the Ag interlayer on the bottom ITO layer (42 nm). (a) ITO (42 nm) single layer, (b) Ag (5 nm)/ITO (42 nm), (c) Ag (10 nm)/ITO (42 nm), (d) Ag (15 nm)/ITO (42 nm), (e) Ag (20 nm)/ITO (42 nm) films.

TABLE III. Maximum optical transmittance, minimum sheet resistance and largest FOM of IAI films reported in the literature.

No.	IAI film	T_{max} at 550 nm (%)	$T_{average}$ (400-800nm) (%)	Sheet resistance (Ω/sq)	FOM (10^{-3} Ω^{-1})	Preparation method	Reference
1	IAI-glass	85		4	49.22	In line sputtering + anneal	Ref. 23
2	IAI-glass	83		5.7	28.3	DC sputtering	Ref. 30
3	IAI-PET	80[a]		16	6.7	DC sputtering	Ref. 31
4	IAI-glass	80.3		23	4.85	RF sputtering	Ref. 32
5	IAI-PET	81	74	11	11.05	DC sputtering	Ref. 33
6	IAI-glass	80		4	26.84	DC sputtering + anneal	Ref. 34
7	IAI-glass	86.63[a]	83.11	6.33	37.61	DC sputtering + anneal	Ref. 35
8	IAI-glass	86[a]		4.4	49.43	DC sputtering	Ref. 36
9	IAI-glass	$>90_{(600nm)}$		4	>90	In line sputtering	Ref. 37
10	IAI-PES	89.28		4.28	75.03	Roll-to-roll sputtering	Ref. 38
11	IAI-glass	79.4[a]		8.9	11	DC&RF sputtering	Ref. 40
12	IAI-PET	83.2[a]		6.7	24	DC&RF sputtering	Ref. 41
13	IAI-glass	78		7	29.13	RF sputtering	Ref. 42
14	IAI-GaN	88		9.21	31.7	RF sputtering + anneal	Ref. 43
15	IAI-glass	85.3		4.46	45.73	DC sputtering	Ref. 44
16	IAI-PET	88.17		3.03	93.71	Roll-to-roll sputtering	Ref. 45
17	IAI-PET	82.4		8.93	16.18	Roll-to-roll sputtering	Ref. 46
18	IAI-glass	91				DC sputtering + etch	Ref. 47
19	IAI-glass	93.12[a]	84.34	6.06	80.9	RF sputtering	Present work

[a]T_{max} chosen from the measured wavelength region.

our sample is also higher than other results of IAI trilayer films on glass substrate at room temperature (except that reported in Ref. 37). This makes it necessary to obtain a low sheet resistance but also maintain a high optical transmittance just by a room-temperature sputtering process. Fig. 2 (d) shows that IAI trilayer films can be easily deposited onto various flexible substrates including polyethylene terephthalate (PET) plastic, a textile and paper. All examples did not have any other treatment but had highly electric conductance.

To further explain the effect of Ag interlayer on the electrical and optical properties of the IAI trilayer electrodes, Fig. 3 shows the SEM images of Ag/ITO (42 nm) bilayer films. Here, Ag films with d_{Ag} = 0, 5, 10, 15 and 20 nm were deposited on the ITO bottom layer film at room temperature. It is obvious to see that the surface morphology of Ag layer was critically dependent on its thickness. When d_{Ag} = 5 nm, Ag island-like particles randomly distributes at the surface of ITO film, as shown in Fig. 3 (b). As a consequence, the ITO layer was not completely covered by Ag layer, leading to the degradation of electrical and optical performance. With increasing d_{Ag}, Ag islands began to connect with each other, finally to form a continuous film. As d_{Ag} = 20 nm, Ag was completely covered the bottom ITO film. This will increase the reflection of light and thus reduce the optical transmittance, although thicker Ag layer increases the electric conductance of IAI electrodes. Only if Ag grains efficiently interconnect with each other on the bottom ITO layer, could IAI films show excellent optical and electric properties.

Fig. 4 shows the AFM images of ITO (48 nm) /Ag/ITO (42 nm) trilayer film as a function of the thickness d_{Ag} of Ag layer. The AFM image of ITO single-layer film (90 nm) was also given for comparison. Firstly, the root mean square (RMS) value of ITO film is very close to 2.84 nm measured in Ref. 28. It is known that a lot of nano-tips and nano-needles occur easily at the surface of ITO films on glass substrate to enhance the surface roughness, especially with none of heating process. Ag interlayer could act as a buffer layer due to its large surface energy, leading to a smaller RMS value of IAI trilayer films. As d_{Ag} increases, the RMS value firstly decreases from 0.75 to 0.65 nm since island-like Ag particles gradually becomes a maze-structure Ag film. However, the even thicker Ag interlayer film would increase the surface roughness of IAI films. The reason may be that the released stress of the thicker Ag film would cause particle reformation. The surface roughness of TCLs films, which plays an important role in determining the device efficiency, could

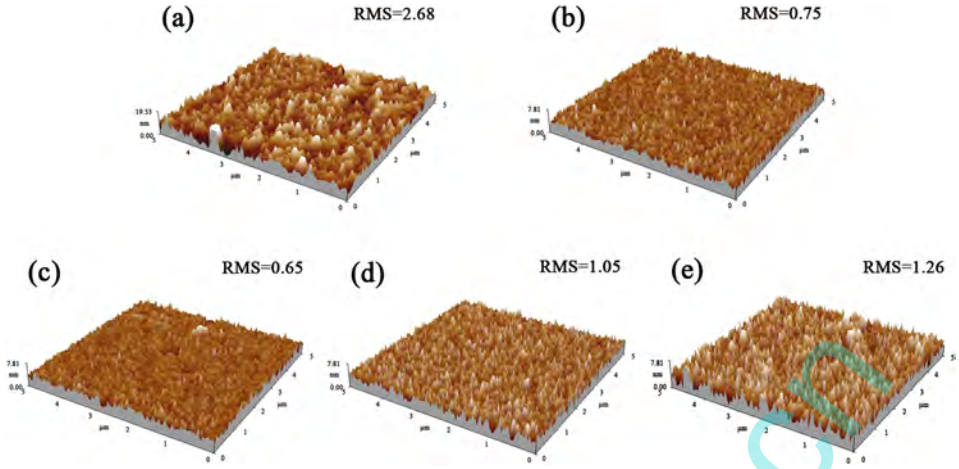

FIG. 4. AFM images of (a) ITO (90 nm) single layer, (b) ITO (48 nm) /Ag (5 nm)/ITO (42 nm), (c) ITO (48 nm) /Ag (10 nm)/ITO (42 nm), (d) ITO (48 nm) /Ag (15 nm)/ITO (42 nm), (e) ITO (48 nm) /Ag (20 nm)/ITO (42 nm) films.

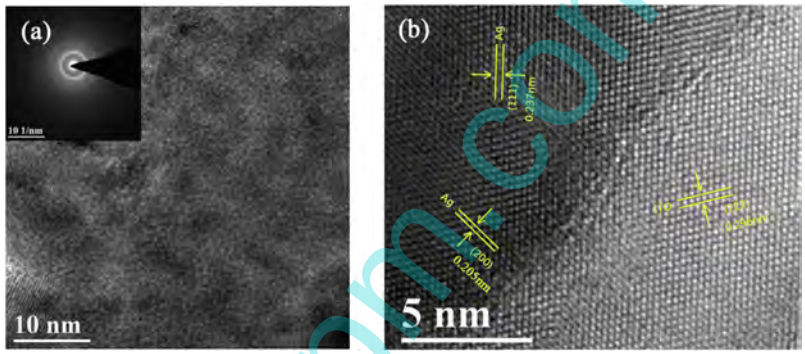

FIG. 5. High resolution electron micrographs (TEM) of IAI films. Insect: Selected area electron diffraction (SAED) pattern.

be improved significantly if introducing a trilayer structure. This result is beneficial for further device fabrication.

Fig. 5 shows the TEM images of the ITO (48 nm) /Ag (5 nm)/ITO (42 nm) trilayer sample which was dispersed in ethanol and placed it on a TEM Cu-grid. In general, the microstructure of the ITO films sputtered at room temperature is an amorphous or a nano-crystalline embedded amorphous structure. Our sample shows a polycrystal structure which can be seen from the selected area electron diffraction (SAED) pattern inserted in Fig. 5 (a). The island-like Ag particles (the dark regions) and the ITO films (the bright regions) were clearly observed in Fig. 5 (a). Furthermore, the enlarged image indicates that the ITO layers grow on a preferential orientation along the (222) direction, where the d spacing between lattice planes is 0.296 nm. The Ag grains grow along the (111) and (200) directions and the d spacing between lattice planes are 0.296 nm and 0.237 nm, respectively.

IV. CONCLUSION

IAI trilayer films were deposited on glass substrate at room temperature by RF magnetron sputtering. The structural, optical and electric properties were greatly influenced by the thicknesses of Ag layer as well as different ITO layers. Sheet resistance as low as 4.88 Ω/sq and high transmittance over 90% were achieved for IAI films with Ag interlayer thickness from 12.5 to 17.5 nm. As Ag interlayer became thicker, the sheet resistance always decreases but the optical transmittance reduces over the visible spectrum. The IAI trilayer electrodes with Ag interlayer thickness between 12.5 and 17.5 nm have similar FOM values (78.59, 80.9 and 77.63×10^{-3} Ω^{-1}). The maximum of FOM value ($80.9\ 10^{-3}$ Ω^{-1}) of the IAI trilayer films was obtained at d_{Ag} = 15 nm. From the morphology and

structural characterization, IAI films show an excellent correlated electric and optical performance in the case that Ag grains interconnect with each other on the bottom ITO layer. The AFM images also demonstrate that IAI films have a very smooth surface which is beneficial for further device application. It is noteworthy that if the thickness of Ag interlayer is less than 5 nm, Ag island-like particles instead of a continuous film will be deposited on the ITO film, leading to the degradation of electric conductance.

ACKNOWLEDGMENTS

This work was supported by the National Natural Science Foundation of China (No. 61464009) and the Major Fundamental Research Program of Inner Mongolia Autonomous Region (No. 20130902).

[1] X. Yu, T. J. Marks, and A. Facchetti, Nature Mater. **15**, 383 (2016).
[2] M. Hala, S. Fujii, A. Redinger, Y. Inoue, G. Rey, M. Thevenin, V. Depredurand, T. P. Weiss, T. Bertram, and S. Siebentritt, Prog. Photovolt: Res. Appl. **23**, 1630 (2015).
[3] H. Belkhalfa, H. Ayed, A. Hafdallah, M. S. Aida, and R. T. Ighil, Optik **127**, 2336 (2016).
[4] J. Y. Lee, S. T. Connor, Y. Cui, and P. Peumans, Nano. Lett **8**, 698 (2008).
[5] J. S. Shiau, S. Brahma, C. P. Liu, and J. L. Huang, Thin Solid Films **620**, 170 (2016).
[6] C. Singh and E. Panda, RSC Adv. **6**, 48910 (2016).
[7] Q. Gao, H. Jiang, C. J. Li, Y. P. Ma, X. Li, Z. H. Ren, Y. Liu, C. L. Song, and G. R. Han, J. Alloys Compounds **574**, 427 (2013).
[8] S. Bae, H. Kim, Y. Lee, X. F. Xu, J. S. Park, Y. Zheng, J. Balakrishnan, T. Lei, H. R. Kim, Y. I. Song, Y. J. Kim, K. S. Kim, B. Ozyilmaz, J. H. Ahn, B. H. Hong, and S. Iijima, Nat. Nanotechnol. **5**, 574 (2010).
[9] N. Fukaya, D. Y. Kim, S. Kishimoto, S. Noda, and Y. Ohno, ACS Nano **8**, 3285 (2014).
[10] Y. Ahn, Y. Jeong, D. Lee, and Y. Lee, ACS Nano **9**, 3125 (2015).
[11] A. Kim, Y. Won, K. Woo, S. Jeong, and J. Moon, Adv. Funct. Mater. **24**, 2462 (2014).
[12] T. Araki, J. Jiu, M. Nogi, H. Koga, S. Nagao, T. Sugahara, and K. Suganuma, Nano Res. **7**, 236 (2014).
[13] M. M. Menamparambath, C. M. Ajmal, K. H. Kim, D. Yang, J. Roh, H. C. Park, C. Kwak, J. Y. Choi, and S. Baik, Sci. Rep **5**, 16371 (2015).
[14] H. W. Tien, S. T. Hsiao, W. H. Liao, Y. H. Yu, F. C. Lin, Y. S. Wang, S. M. Li, and C. C. M. Ma, Carbon **58**, 198 (2013).
[15] U. S. Department of the Interior and U.S. Geological Survey, Mineral Commodity Summaries 80 (2016).
[16] C. Wang, Y. L. Mao, and X. B. Zeng, Appl. Phys. A **110**, 41 (2013).
[17] G. J. Fang, D. J. Li, and B. L. Yao, J. Phys. D: Appl. Phys. **35**, 3096 (2002).
[18] Y. J. Chung, U. K. Kim, E. S. Hwang, and C. S. Hwang, Appl. Phys. Lett. **105**, 013508 (2014).
[19] C. Guillen and J. Herrero, J. Phys. D: Appl. Phys. **46**, 295302 (2013).
[20] Y. H. Lin and C. Y. Liu, J. Electron. Mater. **38**, 108 (2009).
[21] E. Bertran, C. Corbella, M. Vives, A. Pinyol, C. Person, and I. Porqueras, Solid State Ionics **165**, 139 (2003).
[22] C. Guillen and J. Herrero, Thin Solid Films **520**, 1 (2011).
[23] E. Kusano, J. Kawaguchi, and K. Enjouji, J. Vac. Sci **4**, 2987 (1986).
[24] D. R. Sahu and J. L. Huang, Mater. Sci. Eng., B **130**, 295 (2006).
[25] J. H. Kim, Y. J. Moon, S. K. Kim, Y. Z. Yoo, and T. Y. Seong, Ceram. Int. **41**, 14805 (2015).
[26] H. J. Lee, J. W. Kang, S. H. Hong, S. H. Song, and S. J. Park, ACS Appl. Mater. Interfaces **8**, 1565 (2016).
[27] S. H. Yu, L. X. Li, X. S. Lyu, and W. F. Zhang, Sci. Rep. **6**, 20399 (2016).
[28] S. W. Liu, T. H. Su, P. C. Chang, T. H. Yeh, Y. Z. Li, L. J. Huang, Y. H. Chen, and C. F. Lin, Organ. Electron. **31**, 240 (2016).
[29] H. S. Roh, S. H. Cho, and W. J. Lee, Phys. Stat. Sol. A **207**, 1558 (2010).
[30] M. Bender, W. Seelig, C. Daube, H. Frankenberger, B. Ocker, and J. Stollenwerk, Thin Solid Films **326**, 67 (1998).
[31] M. Fahland, P. Karlsson, and C. Charton, Thin Solid Films **392**, 334 (2001).
[32] E. Bertran, C. Corbella, M. Vives, A. Pinyol, C. Person, and I. Porqueras, Solid State Ionics **165**, 139 (2003).
[33] Y. Li, L. D. Wang, C. Chang, L. Duan, and Y. Qiu, Chin. Sci. Bulletin **49**, 1328 (2004).
[34] Y. L. Choi and S. H. Kim, Solid State Phenom. **124**, 403 (2007).
[35] L. Zhang, J. S. Yu, J. Zhong, H. Wang, Y. D. Jiang, and J. F. Deng, Adv. Opt. Manufact. Technol. **6722**, 6722Q-1 (2007).
[36] J. A. Jeong and H. K. Kim, Sol. Energy Mater. Sol. Cells **93**, 1801 (2009).
[37] C. Guillen and J. Herrero, Sol. Energy Mater. Sol. Cells **92**, 938 (2008).
[38] Y. S. Park, K. H. Choi, and H. K. Kim, J. Phys. D: Appl. Phys. **42**, 235109 (2009).
[39] A. Indluru and T. L. Alford, J. Appl. Phys. **105**, 123528 (2009).
[40] T. H. Kim, B. H. Choi, J. S. Park, S. M. Lee, Y. S. Lee, and L. S. Park, Mol. Cryst. Liq. Cryst. **520**, 209 (2010).
[41] T. H. Kim, C. H. Kim, S. K. Kim, Y. S. Lee, and L. S. Park, Mol. Cryst. Liq. Cryst. **532**, 112 (2010).
[42] C. H. Hong, Y. J. Jo, H. A. Kim, I. H. Lee, and J. S. Kwak, Thin Solid Films **519**, 6829 (2011).
[43] J. H. Lee, K. Y. Woo, K. H. Kim, H. D. Kim, and T. G. Kim, Opt. Lett. **38**, 5055 (2013).
[44] H. J. Kim, K. W. Seo, H. K. Yong, J. Choi, and H. K. Kim, Appl. Surf. Sci. **328**, 215 (2015).
[45] S. H. Park, S. J. Lee, J. H. Lee, J. Kal, J. Hahn, and H. K. Kim, Org. Electron. **30**, 112 (2016).
[46] T. H. Kim, S. H. Park, D. H. Kim, Y. C. Nah, and H. K. Kim, Sol. Energy Mater. Sol. Cells **160**, 203 (2017).
[47] K. P. Sibin, N. Selvakumar, A. Kumar, A. Dey, N. Sridhara, H. D. Shashikala, A. K. Sharma, and H. C. Barshilia, Sol. Energy **141**, 118 (2017).
[48] G. Haacke, J. Appl. Phys. **47**, 4086 (1976).